

Enhanced photoelectrochemical activity of vertically aligned ZnO-coated TiO₂ nanotubes

Hua Cai,¹ Qin Yang,¹ Zhigao Hu,² Zhihua Duan,² Qinghu You,¹ Jian Sun,¹ Ning Xu,¹ and Jiada Wu^{1,a)}

¹Department of Optical Science and Engineering, Fudan University, Shanghai 200433, China

²Department of Electronic Engineering, East China Normal University, Shanghai 200241, China

(Received 3 January 2014; accepted 18 January 2014; published online 6 February 2014)

Vertically aligned ZnO-TiO₂ hetero-nanostructures constructed of anatase TiO₂ nanotubes (NTs) and wurtzite ZnO coatings are fabricated by atomic layer deposition of ZnO coatings on electrochemical anodization formed TiO₂ NTs, and their photoelectrochemical activities are studied through photoelectrochemical and electrochemical characterization. Compared with bare TiO₂ NTs, the transient photocurrent increases to over 1.5-fold for the annealed ZnO-coated TiO₂ NTs under visible illumination. The ZnO-coated TiO₂ NTs also show a longer electron lifetime, a lower charge-transfer resistance and a more negative flat-band potential than the bare TiO₂ NTs, confirming the improved photoelectrochemical activity due to the enhanced charge separation. © 2014 AIP Publishing LLC. [<http://dx.doi.org/10.1063/1.4863852>]

Nanostructured TiO₂ and ZnO have recently attracted much attention because of their potential applications such as photocatalytic reactions and photovoltaic processes.¹⁻³ Both metal oxides have advantages of low cost, stability, nontoxicity, and ease of availability. In addition, the good compatibility between TiO₂ and ZnO allows them to be composed as a hetero-nanostructure. Compared with the single oxides, heterostructures constructed from nanostructured TiO₂ and ZnO can provide better performance when used as a photocatalyst or a photoelectrode due to the combination of the high reactivity of TiO₂ and the large binding energy of ZnO, as well as, the staggered band alignment of the formed heterostructures.⁴⁻⁶ An extended range of photoresponse and an enhanced photoactivity can be achieved compared with the single metal oxides, which are most favorable for photocatalytic and photovoltaic applications.⁷⁻¹¹ Much work has been devoted to nano-scaled ZnO-TiO₂ heterogeneous structures, in particular, to one-dimensional hetero-nanostructures including nanotubes (NTs) and nanowires.⁸⁻¹¹

In this work, we fabricated vertically aligned ZnO-coated TiO₂ (ZnO/TiO₂) NTs by electrochemical anodization (EA) of Ti foils followed by atomic layer deposition (ALD) of ZnO. After morphology characterization, photoelectrochemical and electrochemical properties were studied in detail. Photocurrent (PC) density, electrochemical impedance spectroscopy (EIS), and flat-band potential were measured to understand the suppressed electron-hole recombination and the enhanced photoelectrochemical activity of the hetero-nanostructures composed of TiO₂ nanotubes and ZnO coatings and to obtain the improved photoelectrochemical performance.

TiO₂ NTs were first formed on Ti foil (99.99% in purity, 0.1 mm in thickness) by EA. The polished Ti foil was anodized at 0 °C in a two-electrode electrochemical cell using

the Ti foil as the working electrode and a graphite sheet as the counter electrode in 0.5 wt. % HF electrolyte at a voltage of 20 V for 40 min. The formed TiO₂ NTs were then annealed at 450 °C for 3 h in air. The annealed TiO₂ NTs were used as templates for the deposition of ZnO coatings by ALD (TFS200, BENEQ) using diethylzinc [Zn(C₂H₅)₂, DEZ] as the metal precursor and de-ionized water (H₂O) as the reactant. The ZnO coatings were typically deposited at 200 °C by several DEZ-H₂O cycles in the sequence of 0.5-s DEZ pulse, 2-s N₂ purge, 0.5-s H₂O pulse, and 2-s N₂ purge. One-cycle deposit of ZnO is approximately 0.2 nm in thickness when being deposited on a plane substrate. The obtained ZnO/TiO₂ samples were annealed at 450 °C for 30 min in air.

The sample morphology was examined by field-emission scanning electron microscopy (FESEM, Hitachi S-4800), revealing that highly ordered and vertically aligned TiO₂ NTs having an average diameter of ~60 nm and a wall thickness of ~15 nm were formed on Ti foil by EA, as shown in Fig. 1(a). Figure 1(b) shows the planar and cross-sectional FESEM images of ZnO/TiO₂ NTs fabricated by depositing 10 cycles of ZnO on TiO₂ NTs. It can be seen that the TiO₂ NTs are uniformly covered by the ZnO coatings, forming ZnO-coated TiO₂ NTs which have smaller diameters and thicker walls than the bare TiO₂ NTs. No changes in morphology were observed after annealing.

The sample structure was characterized by X-ray diffraction (XRD, Rigaku D/max-γ B X-ray), revealing that the fabricated ZnO/TiO₂ NTs are constructed from nearly tetragonal anatase TiO₂ and hexagonal wurtzite ZnO, as shown in Fig. 2(a), which is dominated by a prominent peak attributed to the (101) diffraction of anatase TiO₂ [A (101)] (JCPDS 21-1272) in addition to the peaks diffracted from Ti foil (denoted by T). Some weak diffraction from wurtzite ZnO (denoted by W) (JCPDS: 36-1451) also appear in the XRD patterns of the ZnO/TiO₂ NTs. Post-fabrication annealing resulted in an improvement in the structures of TiO₂ and ZnO, as revealed by the intensity increase of the diffractions.

^{a)} Author to whom correspondence should be addressed. Electronic mail: jdwu@fudan.edu.cn

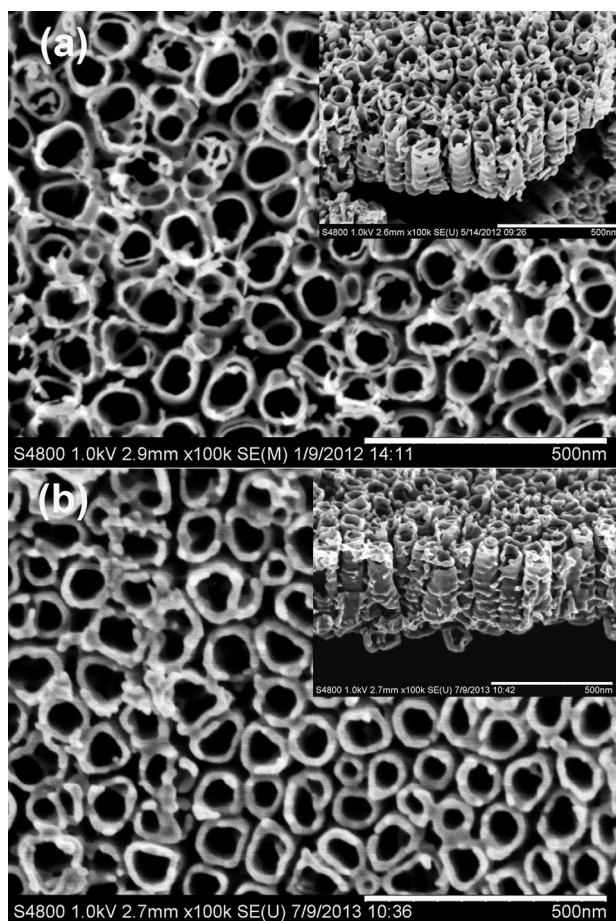


FIG. 1. Top-view and cross-sectional SEM images of bare TiO₂ NTs (a) and ZnO/TiO₂ NTs (b).

The crystal structures of TiO₂ and ZnO and the improvements in the structures were confirmed through the analysis of vibrational modes obtained by Raman scattering measurements (Jobin-Yvon LabRAM HR 800 UV) using a 325-nm He-Cd laser beam to excite the samples. As shown in Fig. 2(b), the Raman spectrum of the as-fabricated ZnO/TiO₂ NTs is similar with that of the bare TiO₂ NTs, both exhibit characteristic Raman modes of anatase TiO₂ (denoted by A).¹² For the annealed sample, however, the Raman mode associated with longitudinal optical (LO) phonons of wurtzite ZnO [A₁(LO)], and its overtones [A₁(2LO) and A₁(3LO)] predominate the spectrum.¹³

With an active area of 1 cm², bare TiO₂ NTs or ZnO/TiO₂ NTs were used as the working photoelectrode and subjected to the irradiation of visible light (100 mW/cm²) for PC measurements in a three-electrode cell in 0.5 M Na₂SO₄ using a CHI electrochemical analyzer (CHI 660A). A Xe lamp was used as the light source to provide visible light by cutting ultraviolet (UV) light using a high-pass filter with a cutoff of 380 or 420 nm. Fig. 3 compares the transient photocurrent response of ZnO/TiO₂ over several on-off cycles of intermittent visible illumination with that of bare TiO₂. For the as-fabricated ZnO/TiO₂ NTs, the photoelectrochemical activity is equal to or smaller than that of the bare TiO₂ NTs under the irradiation by 380-nm or 420-nm cutoff visible light, not as expected. After annealing, in contrast, a significant enhancement in photoelectrochemical activity is

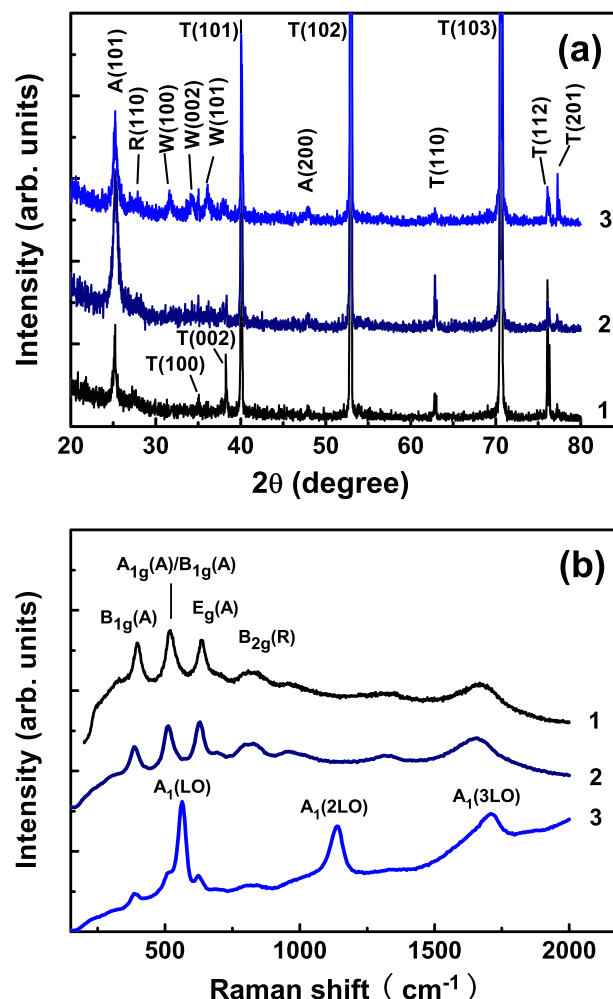


FIG. 2. XRD (a) and Raman spectra (b) of bare TiO₂ NTs (1), as-fabricated ZnO/TiO₂ NTs (2) and annealed ZnO/TiO₂ NTs (3).

observed, suggesting a more efficient separation of photo-generated electron–hole pairs. Post-fabrication annealing improved the quality of the interfaces between ZnO and TiO₂, as well as the structures of ZnO and TiO₂, which should be favorable for the transport and separation of photo-generated electrons and holes. Under the irradiation by 420-nm cutoff visible light, in particular, the PC density increases from $\sim 1.4 \mu\text{A}/\text{cm}^2$ for the bare TiO₂ NTs to $\sim 2.2 \mu\text{A}/\text{cm}^2$ for the annealed ZnO/TiO₂ NTs. The hetero-structured ZnO/TiO₂ NTs have therefore a photoelectrochemical activity of nearly 60% higher than that of the bare TiO₂ NTs. The transient PC density curves illustrated in Fig. 3 also demonstrate that the fabricated ZnO/TiO₂ NTs have a fast photoresponse speed and reasonably good photostability when used as photoelectrodes. Of more practical importance is the significant enhancement in the photoresponse to the light with longer wavelengths, indicating an extended region of photoresponse and a better match with solar spectrum due to the presence of ZnO coatings.

EIS and flat-band potential measurements were performed with a Potentionstat/Galvanostat (EG & G, 273 A) and a two-phase lock-in amplifier (EG & G, 5210). The impedance measurements were carried out at 0.0 V vs the reference electrode Ag/AgCl with frequencies ranging from 100

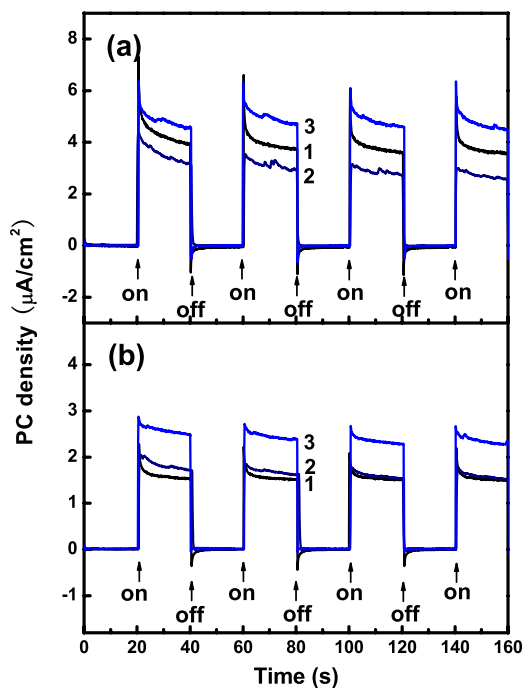


FIG. 3. Transient PC densities of bare TiO_2 NTs (1), as-fabricated ZnO/TiO_2 NTs (2), and annealed ZnO/TiO_2 NTs (3) under visible illumination with cutoff of 380 nm (a) and 420 nm (b).

kHz to 0.1 Hz. Typical EIS Nyquist plots of the bare TiO_2 NTs and the as-fabricated and annealed heterostructured ZnO/TiO_2 NTs are illustrated in Fig. 4(a). It can be seen that with the presence of the ZnO coatings, the ZnO/TiO_2 NTs present a decrease in charge-transfer resistance (R_{ct}), as implied by the smaller value of the arc diameter in Nyquist plot compared to the bare TiO_2 NTs.¹⁴ The charge-transfer resistance controls the kinetics at the electrodes.^{15,16} The smaller R_{ct} reveals the enhanced separation efficiency of photogenerated charge carriers for the ZnO/TiO_2 NTs compared with the bare TiO_2 NTs. With the R_{ct} decreasing, the transfer of charges across the interface between the semiconductor and the solution becomes easier, leading to the increase in the photocurrent, consistent with the results of the PC measurements.

The Bode phase plots in Fig. 4(b) show the characteristic frequency peak of the bare TiO_2 NTs and the heterostructured ZnO/TiO_2 NTs. According to the EIS model,^{17,18} the lifetime (τ_e) of injected electrons can be deduced from the position of the low frequency peak through the expression $\tau_e = 1/(2\pi f_{\text{max}})$, where f_{max} is the frequency at the top of the low frequency arc. The frequency peak of the ZnO/TiO_2 NTs moves to a lower frequency compared with that of the bare TiO_2 NTs. That is to say, the electrons in the ZnO/TiO_2 electrode have a longer lifetime ($\sim 250 \mu\text{s}$) than those in the bare TiO_2 NTs electrode ($\sim 20 \mu\text{s}$). The longer lifetime is ascribed to the high electron mobility of the ZnO/TiO_2 nano-heterostructure,¹⁹ implying a lower recombination rate and an increased separation of charge carriers.

The flat-band potential was determined by the Mott-Schottky analysis method at a scanning rate of $50 \text{ mV}\cdot\text{S}^{-1}$ with a potential range from -1.0 to 1.5 V at 100 Hz . Fig. 4(c) displays the Mott-Schottky plots of the bare TiO_2 NTs and

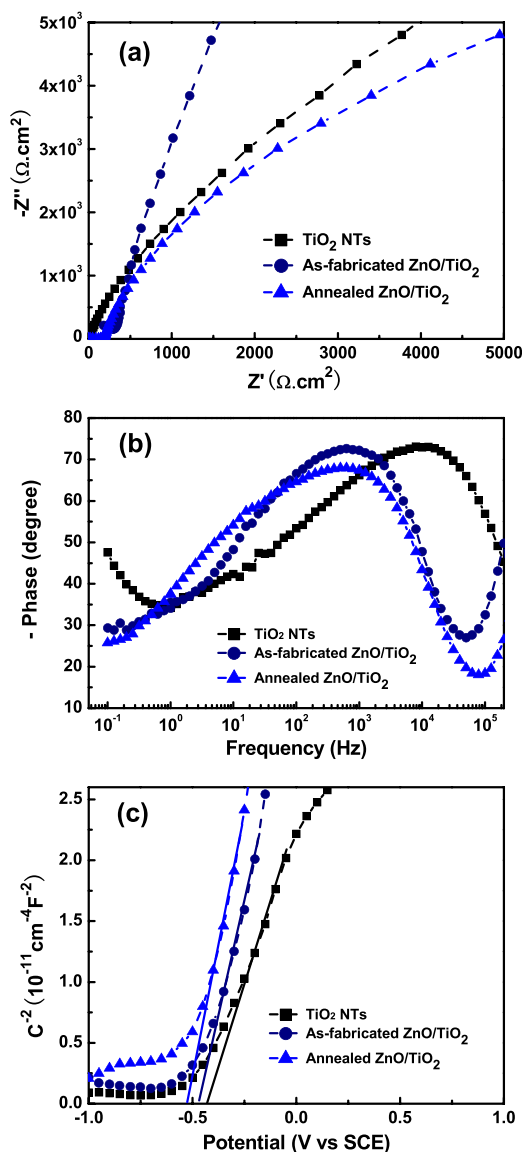


FIG. 4. Nyquist (a), Bode phase (b), and Mott-Schottky (c) plots of bare TiO_2 , as-fabricated ZnO/TiO_2 NTs and annealed ZnO/TiO_2 NTs electrodes in $0.5 \text{ M Na}_2\text{SO}_4$.

the ZnO/TiO_2 NTs. The flat-band potential (V_{fb}) was determined by intersecting the tangent of Mott-Schottky curves with the potential axis.¹⁴ Compared with the bare TiO_2 NTs, V_{fb} shifts negatively for the ZnO/TiO_2 NTs whether annealed or not. The value of V_{fb} for the annealed ZnO/TiO_2 NTs shifts to -0.53 V compared with -0.42 V for the bare TiO_2 NTs, revealing a smaller barrier for charge transfer in the heterostructured ZnO/TiO_2 NTs, which is consistent with the above photoelectrochemical and electrochemical measurements. The V_{fb} plays an important role in photoelectrochemical performance. With a more negative V_{fb} , a higher open-circuit voltage can be expected when used as the photoelectrode in a photovoltaic device.

In conclusion, $\text{ZnO}-\text{TiO}_2$ heterogeneous structures in the form of vertically aligned ZnO-coated TiO_2 nanotubes were fabricated by atomic layer deposition of ZnO coatings on electrochemical anodization formed TiO_2 nanotubes. The hetero-nanostructures are composed of anatase TiO_2 nanotubes and wurtzite ZnO coatings. Compared with the

bare TiO₂ NTs, the transient photocurrent increases to about 1.6 times for the annealed ZnO/TiO₂ NTs under visible illumination, indicating an enhancement in the photoelectrochemical activity. This can be explained in terms of improved charge separation in the ZnO/TiO₂ NTs, which was confirmed by electrochemical characterization. The longer electron lifetime, the lower electron transport resistance, and the more negative flat-band potential of the heterostructured ZnO/TiO₂ NTs are favorable for electron transport with less diffusive hindrance, leading to the suppression in electron-hole recombination and the improvement in photoelectrochemical properties.

This work was supported by the National Basic Research Program of China (No. 2012CB934303), the National Natural Science Foundation of China (No. 11275051), and the Doctoral Fund of Chinese Ministry of Education (No. 20110071110020). The authors thank Professor X. L. Cui for her helpful discussion and Mr. P. Zhao for his assistance in measurements.

¹A. Hagfeldt, G. Boschloo, L. C. Sun, L. Kloo, and H. Pettersson, *Chem. Rev.* **110**, 6595 (2010).

²W. Krenkvirat, S. Sreekantan, A. F. M. Noor, N. Negishi, G. Kawamura, H. Muto, and A. Matsuda, *Mater. Chem. Phys.* **137**, 991 (2013).

- ³J. H. Lee, J. H. Shin, J. Y. Song, W. F. Wang, R. Schlaf, K. J. Kim, and Y. Yi, *J. Phys. Chem. C* **116**, 26342 (2012).
- ⁴P. Reiss, M. Protiere, and L. Li, *Small* **5**, 154 (2009).
- ⁵J. van Embden, J. Jasieniak, D. E. Gomez, P. Mulvaney, and M. Giersig, *Aust. J. Chem.* **60**, 457 (2007).
- ⁶Z. M. Wu, Y. Zhang, J. J. Zheng, X. G. Lin, X. H. Chen, B. W. Huang, H. Q. Wang, K. Huang, S. P. Li, and J. Y. Kang, *J. Mater. Chem.* **21**, 6020 (2011).
- ⁷V. Manthina, J. P. C. Baena, G. L. Liu, and A. G. Agrios, *J. Phys. Chem. C* **116**, 23864 (2012).
- ⁸Y. L. Xie, Z. X. Li, Z. G. Xu, and H. L. Zhang, *Electrochem. Commun.* **13**, 788 (2011).
- ⁹F. X. Xiao, *ACS Appl. Mater. Interfaces* **4**, 7055 (2012).
- ¹⁰R. Liu, W. D. Yang, L. S. Qiang, and H. Y. Liu, *J. Power Sources* **220**, 153 (2012).
- ¹¹J. S. Jeong, B. H. Choe, J. H. Lee, J. J. Lee, and W. Y. Choi, *J. Electron. Mater.* **43**, 375–380 (2014).
- ¹²S. P. S. Porto, P. A. Fleury, and T. C. Damen, *Phys. Rev.* **154**, 522 (1967).
- ¹³J. F. Scott, *Phys. Rev. B* **2**, 1209 (1970).
- ¹⁴A. I. Kontos, V. Likodimos, T. Stergiopoulos, D. S. Tsoukleris, P. Falaras, I. Rabias, G. Papavassiliou, D. Kim, J. Kunze, and P. Schmuki, *Chem. Mater.* **21**, 662 (2009).
- ¹⁵K. Y. Tse, B. M. Nichols, W. S. Yang, J. E. Butler, J. N. Russell, and R. J. Hamers, *J. Phys. Chem. B* **109**, 8523 (2005).
- ¹⁶W. H. Leng, Z. Zhang, J. Q. Zhang, and C. N. Cao, *J. Phys. Chem. B* **109**, 15008 (2005).
- ¹⁷R. Kern, R. Sastrawan, J. Ferber, R. Stangl, and J. Luther, *Electrochim. Acta* **47**, 4213 (2002).
- ¹⁸G. Zhu, Z. J. Cheng, T. Lv, L. K. Pan, Q. F. Zhao, and Z. Sun, *Nanoscale* **2**, 1229 (2010).
- ¹⁹J. F. Qian, P. Liu, Y. Xiao, Y. Jiang, Y. L. Cao, X. P. Ai, and H. X. Yang, *Adv. Mater.* **21**, 3663 (2009).